THE ASTROPHYSICAL JOURNAL, 360:257–266, 1990 September 1

VELOCITY-RESOLVED FAR-INFRARED SPECTRA OF [Fe II]: EVIDENCE FOR MIXING AND CLUMPING IN SN 1987A

MICHAEL R. HAAS,[1] SEAN W. J. COLGAN,[1,2] EDWIN F. ERICKSON,[1] STEVEN D. LORD,[1,3]
MICHAEL G. BURTON,[1,3,4] AND DAVID J. HOLLENBACH[1]
Received 1989 November 22; accepted 1990 February 23

ABSTRACT

We present ~ 400 km s^{-1} resolution profiles of the 17.94 and 25.99 μm [Fe II] transitions from SN 1987A at $t \sim 400$ days after core collapse. These observations used the facility cooled grating spectrometer aboard NASA's Kuiper Airborne Observatory. The two profiles are similar and have FWHM line widths of ~ 2700 km s^{-1}. The higher signal-to-noise 18 μm profile is somewhat asymmetric, falling off more steeply on the redshifted side than on the blue. Gaussian fits to the profiles yield an average centroid velocity of 280 ± 140 km s^{-1} relative to the Large Magellanic Cloud. The wings of the profiles extend to velocities $\gtrsim 3000$ km s^{-1}. This shows that a significant fraction of the iron has been mixed outward into the hydrogen-rich envelope, which has a minimum expansion velocity of 2100–2400 km s^{-1}. Both profiles also contain an unresolved 3–5 σ emission feature on the redshifted wing at $v_{\rm LSR} \sim +3900$ km s^{-1}. We interpret this feature as emission from a high-velocity clump of material containing $\sim 3\%$ of the total iron mass. The total line flux of the 26 μm ground-state transition yields an optically thin, singly ionized iron mass of 0.026 $M_\odot$, relatively independent of the assumed temperature. This is significantly less than the 0.06 $M_\odot$ of Fe^+ determined from the decline of the optical light curve and the ionization of measured nickel lines, implying that the iron transitions still have appreciable optical depth. However, because of the small change in the 26 μm line flux from our measurement at 250 days, and the similarity of our profiles to the 1.26 μm [Fe II] profile, most of the emission is believed to originate from optically thin material with a temperature of 4400 ± 400 K. A comparison of the data with spherically symmetric models indicates a power-law density exponent of -3.2 ± 1.1 and a minimum expansion velocity of 650 ± 650 km s^{-1} for this optically thin component. The [Fe II] line fluxes and profiles also imply that the remainder of the material has high optical depth and is distributed in clumps throughout the ejecta, rather than being concentrated at low velocities in the center of a smooth density distribution.

Subject headings: infrared: spectra — line profiles — stars: abundances — stars: individual (SN 1987A) — stars: supernovae

I. INTRODUCTION

Studies of the far-infrared line emission from SN 1987A have the advantage of revealing the interior structure of the expanding ejecta at earlier epochs than do the ultraviolet or optical transitions. However, the infrared spectral line observations have been confined to $\lambda \lesssim 30$ μm because the maximum possible flux, which is produced in optically thick ejecta, decreases as λ^{-3} (e.g., Colgan and Hollenbach 1988) and because the diameter of the largest suitable telescope, the Kuiper Airborne Observatory (KAO), is only 0.9 m. Nonetheless, these observations have provided a relatively unobstructed view of the heavy element–rich interior of the expanding ejecta. Airborne observations at wavelengths from 5 to 12 μm have yielded detections of nickel, argon, and cobalt emission from the core of the supernova (Rank *et al.* 1988*a*, *b*; Witteborn *et al.* 1988, 1989; Bregman *et al.* 1990) with resolutions of ~ 1500–5000 km s^{-1}. Moseley *et al.* (1987, 1988*a*, *b*, 1989) have used the KAO to detect iron and possibly sulfur transitions between 16 and 30 μm with resolutions of ~ 1100–$10{,}000$ km s^{-1}. Both these groups have also detected hydrogen recombination lines which presumably originate in the overlying hydrogen-rich envelope. Aitken *et al.* (1988*a*) and Bouchet and Danziger (1988) have reported ground-based observations in the 8–13 μm band with resolutions of $\gtrsim 3000$ km s^{-1}. A blend of CO transitions at 2.3 μm (Spyromilio *et al.* 1988) and near-infrared iron and nickel transitions (Spyromilio, Meikle, and Allen 1990) have been observed with a resolution of 200–300 km s^{-1}. We have previously carried out observations of the 26.0 μm [Fe II] transition with ~ 1800 km s^{-1} resolution at 250 days (Erickson *et al.* 1988, hereafter Paper I). Here we present and discuss spectra of the 17.9 and 26.0 μm [Fe II] transitions with a resolution ~ 400 km s^{-1}, which were obtained 400 days after core collapse (see Haas *et al.* 1988). These iron lines are well isolated, and the new spectra have sufficient signal-to-noise and resolution to unambiguously show velocity structure in the expanding ejecta. From our fluxes and line profiles, we conclude that both mixing and clumping are important phenomena in SN 1987A. In § II we outline our observational techniques and present the data. In § III we describe the characteristics of the line profiles, including the evidence for mixing, in § IV we discuss the optical depth distribution, clumping, and temperature of the ejecta, and in § V we present spherically symmetric radiative transfer models which support and extend the conclusions of the earlier sections.

II. OBSERVATIONS

The observations of SN 1987A were made from the Kuiper Airborne Observatory with the facility cooled grating spectrometer developed by Erickson *et al.* (1984*a*, *b*, 1985). The flights originated from Christchurch, New Zealand on the

[1] NASA-Ames Research Center.
[2] The SETI Institute.
[3] NAS National Research Council Research Associate.
[4] University of California, Irvine.

nights of 1988 April 5 and 7; this was 407 and 409 days after the explosion, respectively. Based on the lower resolution measurements of Moseley *et al.* (1988*a*, *b*), we chose the forbidden, fine-structure [Fe II] transitions at 18 and 26 μm for higher resolution study because they were the brightest transitions between 16 and 30 μm at this epoch.

As described in Paper I, the telescope was guided directly on the visual image of the supernova. The telescope secondary was chopped in azimuth (approximately east-west) at a frequency of 32 Hz with an amplitude of 2′. In order to accommodate the broad line widths of SN 1987A, the cooled grating spectrometer was modified to reduce its spectral resolution from $\sim$75 to $\sim$400 km s^{-1}. An array of 13 Si:As BIB photoconductor detectors, similar to those described by Serabyn *et al.* (1988), were kindly provided by Rockwell International. The velocity spacing of the detectors was 380 km s^{-1} at 18 μm and 390 km s^{-1} at 26 μm. The FWHM beamwidths were 22″ at 18 μm and 30″ at 26 μm. The latter beamwidth degraded the velocity resolution at 26 μm to 460 km s^{-1}.

Flux calibration was accomplished through observations of VY CMa (Moseley, private communication; Gezari, Schmidt, and Mead 1987) just prior to each supernova observation. The source η Car (Moseley, private communication; Gezari, Schmidt, and Mead 1987; Harvey, Hoffman, and Campbell 1978) was observed after the supernova and was used as a secondary calibration source. The observed ratio of these two sources agreed with Moseley's fluxes to 10%. There is no significant atmospheric absorption in our bandpass at 18 μm, but at 26 μm there is a water feature with a minimum transmission of $\sim$80% at our resolution. The line-of-sight water vapor was measured in absorption against the calibration sources three times during the April 7 (26 μm) flight. Variations in the water vapor burden were also monitored by an on-board radiometer. The correction for the differential water vapor absorption between the supernova line of sight and the line of sight to the calibration sources was negligible. Thus the primary effect of the water lines was to increase the noise in the affected detectors ($-800 \lesssim v \lesssim 200$ km s^{-1}). The overall uncertainty in the absolute flux calibration is estimated to be $\pm$15%.

Each line was observed using three different wavelength settings—one central position and two positions offset by $\pm$6 detectors so as to adequately cover the broad line and adjacent continuum. The integration time at each wavelength setting was about 45 minutes. The data at each setting were separately calibrated and then combined, yielding a 25 point spectrum covering $\pm$4500 km s^{-1}. The spectra are shown in Figures 1*a* and 1*b*. The unequal error bars reflect the different integration times at the various velocities, variations in the atmospheric transmission, the different noise of each detector, and systematic differences in the fluxes obtained by different detectors at the same velocity.

III. LINE PROFILES

a) The Central Profiles

In this section, we describe the characteristics of the two profiles and conclude that they provide direct evidence for significant mixing of the iron into the hydrogen-rich envelope. We identify the measured line profiles as being due to the Fe$^+$ transitions $a^4F\ J = 9/2$–$a^4F\ J = 7/2$ ($\lambda = 17.936$ μm) and $a^6D\ J = 9/2$–$a^6D\ J = 7/2$ ($\lambda = 25.988$ μm) (Corliss and Sugar 1982). For the 18 μm line, there is no other plausible transition within $\pm$5000 km s^{-1} of our central velocity. As pointed out in Paper I, when allowance is made for the broad widths of the supernova emission lines, there are several other transitions which could contribute to the measured emission at 26 μm. However, these transitions originate in highly ionized species and are not expected to produce significant emission (see Colgan and Hollenbach 1988). Moreover, the excellent agreement between our centroid velocities and widths for the 18 and 26 μm lines strongly suggests that the latter is also due to singly ionized iron. The energy level diagram for [Fe II] is given in Figure 2. It illustrates the relationship between these two transitions and the 1.26 μm transition observed by Spyromilio, Meikle, and Allen (1990).

Table 1 lists the continuum level, the integrated line flux, the peak flux density after subtraction of the continuum, the corresponding velocity, v_{peak}, the centroid velocity, v_{cent}, and the

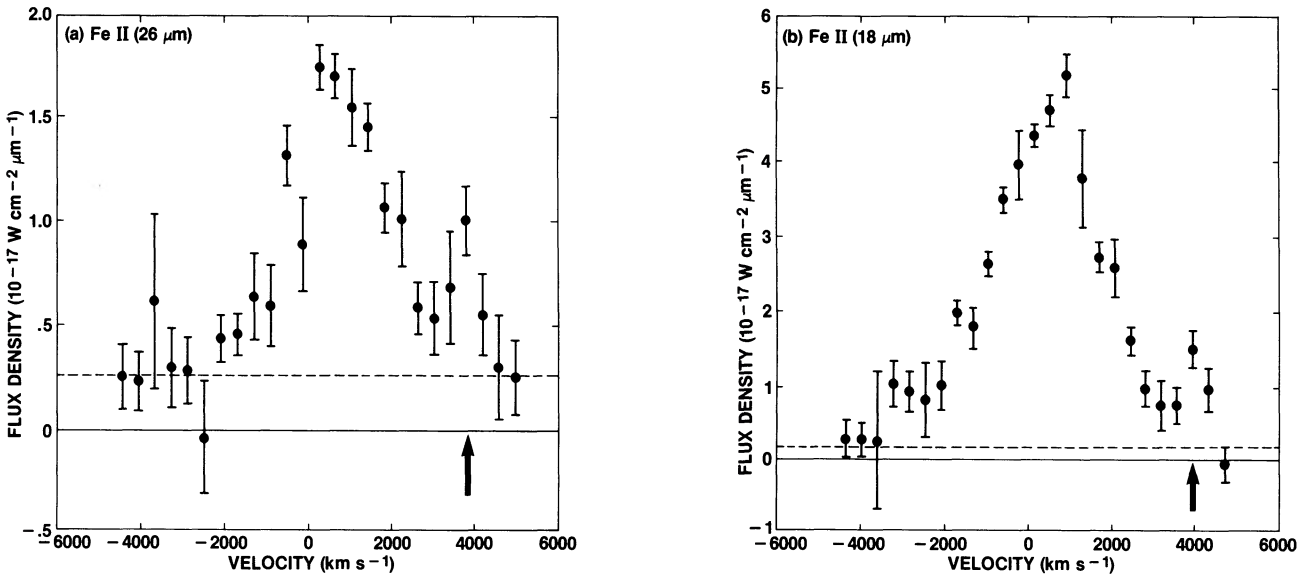

FIG. 1.—[Fe II] 26 μm (*a*) and 18 μm (*b*) spectra of SN 1987A at 407 and 409 days after the event, respectively. The 1 σ error bars are included, and the velocities are relative to the LSR. Adopted continuum levels are indicated by dashed lines, and arrows at $\sim$3900 km s^{-1} highlight the high-velocity emission feature.

TABLE 1

[Fe II] LINE PARAMETERS

Transition (μm)	Continuum (Jy)	Line Flux[a] (10^{-18} W cm^{-2})	Peak Flux Density (10^{-18} W cm^{-2} μm^{-1})	v_{peak}[b] (km s^{-1})	v_{cent}[b] (km s^{-1})	Δv_{FWHM} (km s^{-1})
			Main Profile			
17.9.....	2 ± 2	10.9 ± 0.9	46 ± 3	950 ± 200	450 ± 200[c]	2900 ± 80[c]
26.0.....	6 ± 2	4.3 ± 0.5	15 ± 3	$290 \pm {}^{800}_{200}$	680 ± 200[c]	2500 ± 150[c]
			High-Velocity Feature			
17.9.....	...	0.48 ± 0.10	...	...	4000 ± 200	540 ± 120
26.0.....	...	0.38 ± 0.12	...	...	3800 ± 200	480 ± 150

[a] The errors include statistical errors and $\pm 5\%$ (1σ) absolute calibration uncertainty.
[b] Relative to local standard of rest; errors are uncertainties in the wavelength calibration.
[c] From Gaussian fit to central ± 2500 km s^{-1}.

FWHM velocity width, Δv_{FWHM}, for both profiles. The latter two quantities were obtained from a Gaussian fit to the central ± 2500 km s^{-1} of each profile, thereby avoiding the high-velocity feature at ~ 3900 km s^{-1} (indicated in Fig. 1 and discussed in § III*b*). All velocities are relative to the local standard of rest (LSR). The corresponding parameters for the high-velocity feature are also listed in Table 1.

There is no significant change in the 26 μm line flux since our previous measurement 250 days after the event (Paper I). Including the estimated uncertainties in absolute calibration at both epochs, the flux change is only $-5 \pm 24\%$. The difference in v_{peak} between the two transitions is not significant, since a change in the flux density by $\pm 1\ \sigma$ can shift v_{peak} by the indicated errors. The centroid velocities of the two profiles are also consistent within the errors and give an average value of 565 ± 140 km s^{-1}. This indicates that the emission centroid is redshifted by $\bar{v} = 280 \pm 140$ km s^{-1} relative to the $+285$ km s^{-1} center-of-mass LSR velocity of the supernova determined from circumstellar emission lines (Wampler and Richichi 1989). This redshift relative to the LMC is in reasonable agreement with the ~ 200–600 km s^{-1} resolution observations at 1–5 μm on day 349 (Meikle *et al.* 1989), which yield an average velocity $\bar{v} \sim +500 \pm 80$ km s^{-1}, and with other lower resolution observations at similar epochs. Witteborn *et al.* (1989) attribute this redshift to scattering of the photons by electrons in the expanding hydrogen envelope, whereas Spyromilio, Meikle, and Allen (1990) attribute it to asymmetries in the distribution or temperature of the ejected material.

Figure 1 shows that the central portion of our 18 μm line profile appears somewhat asymmetric, with a steep edge on the redshifted side and a more gradual decline on the blueshifted side. The profile also has v_{cent} significantly different than v_{peak}. Although the 26 μm line shape is consistent with that of the 18 μm line, the lower signal-to-noise prevents us from determining whether the same asymmetry is present. The symmetry in the 18 μm line cannot be produced by electron scattering as described by Witteborn *et al.* (1989). While such scattering could be present and may account for the redshifted centroid velocity, spherically symmetric scattering models predict a steep shoulder on the blue shifted wing and a more gradual decline on the redshifted wing (Witteborn *et al.* 1989; Fransson and Chevalier 1989). This is the opposite of what is observed. Blending with other lines cannot produce the observed shape, since there are no other transitions with wavelengths sufficiently near 17.9 μm which are likely to be strong. There is no sign of the excited state [Ni II] line at 18.24 μm, which lies 5100 km s^{-1} to the red of the 17.9 μm [Fe II] line and is expected to have a similar line width.

We agree with Spyromilio, Meikle, and Allen (1990) that the asymmetry in the profiles and their apparent redshifts are most likely due to asymmetries in the ejecta. Figure 3 compares the central portion of our 18 μm line with a normalized plot of the 1.26 μm Fe^+ line measured by Spyromilio, Meikle, and Allen at 377 days; there has been no shift in the velocity scale. The

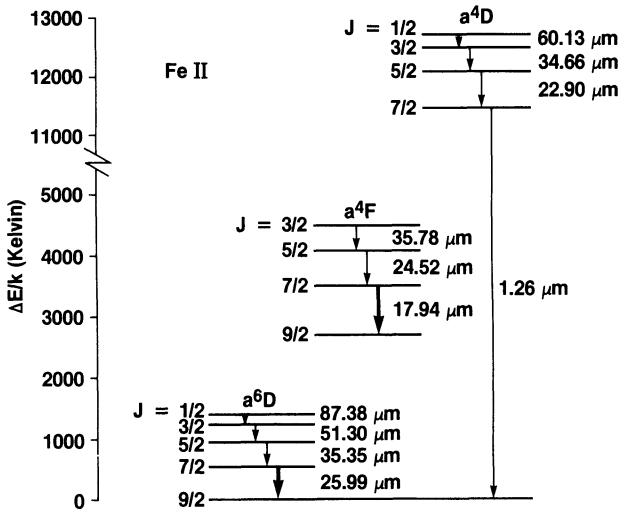

FIG. 2.—Energy level diagram for [Fe II] showing the relationship of the 18 and 26 μm transitions.

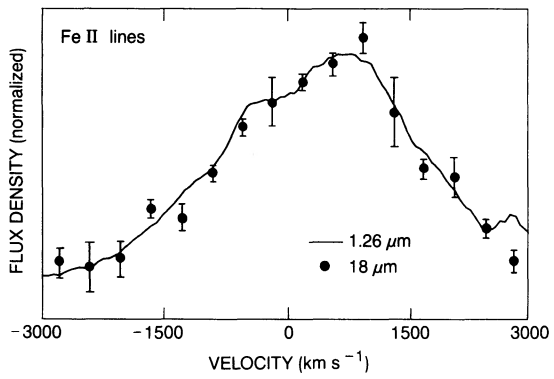

FIG. 3.—A comparison of the central portion of the 18 μm profile at 407 days (*filled circles*) with the normalized 1.26 μm Fe^+ profile of Spyromilio, Meikle, and Allen (1990) at 377 days (*solid curve*).

excellent agreement suggests that the asymmetry results from density, rather than temperature, inhomogeneities because of the extreme temperature sensitivity of the higher excitation 1.26 μm line (Fig. 2). Perhaps the asymmetry is caused by an asymmetric acceleration of the heavy element–rich mantle during the explosion. Polarization observations (Cropper *et al.* 1988) and speckle interferometry (Karovska *et al.* 1988), with models discussed by Chevalier and Soker (1989), indicate that the acceleration of the envelope was also asymmetric. We will use this remarkable similarity between the 18 and 1.26 μm profiles to constrain the optical depth distribution (§ IV*c*) and our radiative transfer models (§ V).

After subtraction of the continuum, we find that at least 20% of the total line flux comes from material with a line-of-sight velocity $|v - v_{\rm cent}| \geq 2000$ km s^{-1} and 10% from material with a line-of-sight velocity $|v - v_{\rm cent}| \geq 3000$ km s^{-1}. As shown below, we detect only $\sim$45% of the total singly ionized iron and the ionization fraction is estimated to be $x_{\rm Fe^+} = 0.8$. The high-velocity material is more likely to be optically thin because its velocity dispersion is higher and its density may be lower (see § V). This means that $\gtrsim$4% of the total iron has a line-of sight velocity $|v - v_{\rm cent}| \geq 3000$ km s^{-1}. This estimate is a lower limit to the amount of material with a large expansion velocity, however, because projection effects mean that some high-velocity material will contribute to the core of the profiles, rather than the wings. For example, if the maximum iron expansion velocity, $v_{\rm exp}$, is as large as 15,000 km s^{-1} (see § V), then $\sim\frac{1}{2}$ the material with $v_{\rm exp} \geq 3000$ km s^{-1} has a line-of-sight velocity $\geq$3000 km s^{-1}, assuming a symmetric expansion and a power-law density distribution (r^{α}) with $-4 \leq \alpha \leq 0$. If the maximum expansion velocity is as small as 4000 km s^{-1}, this fraction decreases to $\sim\frac{1}{8}$. Including this correction, but excluding the (asymmetric) high-velocity feature (§ III*b*), we estimate that from 4%–17% of the total iron mass has an expansion velocity in excess of 3000 km s^{-1}.

The hydrogen envelope has a minimum expansion velocity of +2100 to +2400 km s^{-1} (Woosley 1988; Dopita *et al.* 1988). The presence of significant Fe$^+$ emission at velocities $\gtrsim$2000 km s^{-1} demonstrates that a significant amount of the parent radioactive nickel which eventually decayed to iron was mixed out into the hydrogen-rich envelope during the explosion. This mixing of iron to high velocities can account for the early emergence of X-rays and γ-rays from the supernova (Pinto and Woosley 1988*a*, *b*). Alternatively, Fabian and Rees (1988) have proposed that large holes in the remnant could account for the early emergence of X-rays, the observed X-ray variability, and the emission line at $\sim$6.8 keV without necessitating mixing. However, our spectra provide direct evidence for mixing of the daughter product iron to high velocities. This mixing may have occurred either from instabilities as the shock propagated through the star (Nagasawa, Nakamura, and Miyama 1988; Arnett, Fryxell, and Müller 1989; Ebisuzaki, Shigeyama, and Nomoto 1989) or later in the evolution due to energy from the radioactive decay of ^{56}Ni (Woosley 1988). One or both of these processes may have also contributed to the asymmetries observed in the [Fe II] (18 μm) profile. Our maximum Fe$^+$ velocity of $v_{\rm max} \gtrsim 3000$ km s^{-1} is consistent with the theoretical expectations of $\sim$3000 km s^{-1} velocities for the heavy elements before the deceleration due to the reverse shock propagating back into the mantle (Woosley, Pinto, and Weaver 1988) and the subsequent acceleration to $\sim$4000 km s^{-1} due to the radioactive decay of nickel.

b) The High-Velocity Feature

A high-velocity feature is present in both profiles of Figure 1 at a velocity with respect to the LSR of $\sim +3900$ km s^{-1}. A similar feature may be present on the red wing of the [Co II] (10.52 μm) profile observed by Aitken *et al.* (1988*b*) with a similar spectral resolution. As pointed out by Aitken *et al.*, however, at least part of their feature can be plausibly ascribed to [Ni II]* at 10.68 μm. The high-velocity feature seen in both [Fe II] spectra is also consistent with low-resolution, near-infrared observations of the isolated transitions [Ni II] (6.64 μm) and [Ar II] (6.99 μm), which exhibit an asymmetric wing on the redshifted side (Witteborn *et al.* 1989). When the 18 and 26 μm spectra are degraded to the same resolution as these 7 μm measurements, their asymmetric shape is quite similar to the shorter wavelength profiles at the same epoch. This suggests that the asymmetry of the short-wavelength transitions may be produced, at least in part, by an unresolved high-velocity feature and not simply by broad wings on the red side of the profiles. Finally, this high-velocity feature is certainly present in the profile of this same [Ni II] transition when observed with $\sim$400 km s^{-1} resolution at $\sim$650 days (Colgan *et al.* 1990).

Witteborn *et al.* attribute their line asymmetries to electron scattering in the expanding, partially ionized hydrogen envelope. However, an electron scattering explanation has difficulty accounting for the high-velocity feature, since it has a rapidly changing local maximum which is well separated from the central profile (Pinto, private communication; Witteborn *et al.* 1989; Fransson and Chevalier 1989). Also, the maximum electron expansion velocity deduced by Witteborn *et al.* from their [Ni II] (6.64 μm) line, even including their estimated 20% uncertainty, is only 3600 km s^{-1}. This does not include the full extent of our high-velocity feature. We believe this feature is actually caused by material accelerated to high velocity during or after the explosion, and that electron scattering, while present, is less important than deduced from lower resolution observations. This acceleration could, for example, be due to anisotropic mixing when the radioactive nickel bubble "popped" (Woosley, Pinto, and Weaver 1988).

The parameters of the high-velocity feature are summarized in Table 1. After the adjacent spectrum has been used to remove the continuum and the contribution from the wing of the central profile, we obtain an LSR velocity of 3900 $\pm$ 140 km s^{-1} and a width of 500 $\pm$ 100 km s^{-1} for the average of the 18 and 26 μm features. This width is not significantly larger than our resolution, so the intrinsic line width may be considerably smaller. The 18/26 flux ratio for the high-velocity feature corresponds to a temperature $T = 2600 \pm 900$ K. With this temperature, the flux at 26 μm yields a mass of 0.002 $M_{\odot}$, or about 3% of the total iron mass in the ejecta. The computation of temperatures and iron masses is discussed more fully in the next section.

The high-velocity feature originates in material which has been accelerated away from us, on the far side of the ejecta. However, even if the "mystery spot" seen shortly after the explosion (Nisenson *et al.* 1987; Meikle, Matcher, and Morgan 1987) is real (e.g., Wood *et al.* 1989), it is probably not related. The "mystery spot" requires that a parcel of material be ejected with a velocity in the plane of the sky of at least half the speed of light. Such material would need to have an improbably small-velocity component along the line of sight (within

$\lesssim 2°$ of the plane of the sky) to be related to the high-velocity feature.

IV. DISCUSSION

In this section we discuss the optical depths, clumping, and temperatures inferred for the iron ejecta. In § IV*a* we show that the FIR fluxes, independent of the observed line profiles, also suggest that significant mixing has occurred. In § IV*b* we estimate the average escape probability at 26 μm and conclude that some of the ejecta still has significant optical depth. In § IV*c*, we discuss the optical depth distribution for the ejecta and conclude that most of the measured emission comes from optically thin regions. In § IV*d*, we ratio the two line profiles, show that they are consistent with optically thin emission, and derive a temperature for the ejecta of ~ 4400 K.

a) Evidence for Mixing

As shown in § III*a*, the velocity extent of the FIR line profiles provides direct evidence for mixing of the iron into the hydrogen envelope. Indeed, we can show that the simple theoretical picture in which each element expands at a nearly constant radial velocity in its own thin, onion-like shell (e.g., Fig. 27 of Woosley 1988) implies such large optical depths that emission lines in the infrared would be undetectable. The optical depth through a spherically expanding cloud, averaged over the line profile (the Sobolev approximation, see McCray 1989), is

$$\bar{\tau} = \frac{A\lambda^3 t n_l g_u}{8\pi g_l}\left[1 - e^{-\Delta E/kT}\right], \quad (1)$$

where A is the Einstein A-coefficient, λ is the wavelength, t is the time since the explosion, n_l is the number density in the lower state of the transition, g_u and g_l are the statistical weights of the upper and lower states, ΔE is the energy difference between the upper and lower states, and k is Boltzman's constant. This expression assumes uniform density and homologous ($v_{\rm exp} = r/t$) expansion.

For the 26 μm [Fe II] line with 0.07 $M_\odot$ of singly ionized iron and $T = 4000$ K, equation (1) becomes

$$\bar{\tau} \sim 11.7\left[\left(\frac{v_{\rm max}}{1000\ {\rm km\ s^{-1}}}\right)^3 - \left(\frac{v_{\rm min}}{1000\ {\rm km\ s^{-1}}}\right)^3\right]^{-1} \times \left[\frac{t}{400\ {\rm days}}\right]^{-2}, \quad (2)$$

where $v_{\rm max}$ and $v_{\rm min}$ are the maximum and minimum expansion velocities of the ejected iron shell. For early predictions of $v_{\rm min} = 700$ km s^{-1} and $v_{\rm max} = 1200$ km s^{-1} from unmixed models by Woosley, Pinto, and Ensman (1988), we find $\bar{\tau} = 8.4$ at $t = 400$ days. For a thin expanding shell with negligible velocity shear across the heavy element region (e.g., Woosley 1988) having $v_{\rm min} = 2400$ km s^{-1} and $v_{\rm max} = 2500$ km s^{-1}, we obtain $\bar{\tau} = 6.5$. For $v_{\rm min} = 0$ km s^{-1} and $v_{\rm max} = 2500$ km s^{-1}, $\bar{\tau} = 0.75$.

The escape probability β and the total line flux S are given by

$$\beta = \frac{1 - e^{-\bar{\tau}}}{\bar{\tau}}, \quad (3)$$

and

$$S = \beta S_{\rm thin}, \quad (4)$$

where $S_{\rm thin}$ is the total flux if all the gas is optically thin (e.g., Colgan and Hollenbach 1988). For the above case with 0.07 $M_\odot$ of Fe^+ and $\bar{\tau} = 0.75$, we obtain a flux comparable to that observed, whereas for $\bar{\tau} = 6.5$, the flux is reduced by a factor of 5. This argument is even stronger at $t \sim 250$ days, where the 26 μm line was first detected and has a comparable flux (Paper I). Hence, the infrared transitions from SN 1987A would be expected to be detectable only if the optical depths were sufficiently small so that a significant fraction of the flux escaped. Our models (§ V) show that this conclusion is generally true and does not depend on the assumption of uniform density, as long as the density distribution is not peaked too sharply at low velocities. Sufficiently small optical depths require maximum expansion velocities of $v_{\rm max} \gtrsim 2000$ km s^{-1} and a range of velocities comparable to $v_{\rm max}$, so that $v_{\rm min} \ll v_{\rm max}$. If the density distribution is strongly centrally peaked, then the fluxes are undetectable even when $v_{\rm min}$ and $v_{\rm max}$ satisfy these criteria. Thus we conclude, independent of the detailed shape of the observed profiles, that the heavy elements which have detectable FIR transitions are well mixed into the hydrogen envelope and that a substantial fraction of the mass must be at large velocities. These conclusions are consistent with those deduced from the observed line profiles in § III*a* and our best-fit models in § V.

b) Escape Probability

For our subsequent analysis, we now consider the escape probability implied by our [Fe II] profiles. The initial mass of radioactive nickel has been estimated from the decline of the optical light curve to be 0.065 $M_\odot$ (Woosley, Pinto, and Weaver 1988). After 400 days, the radioactive decay of nickel would have resulted in 0.063 $M_\odot$ of iron. There is an additional 0.01 $M_\odot$ of preexisting iron (Woosley, Pinto, and Weaver 1988). It can easily be shown that the incorporation of even 1% of this iron into dust grains would result in an optical depth $\gg 1$ at visible wavelengths. The lack of a sharp drop in the optical light curve relative to the expected exponential decline from the radioactive decay of nickel (Suntzeff *et al.* 1988; Whitelock *et al.* 1988) indicates that this has not happened (see Gehrz and Ney 1987; Dwek 1988*a*). Furthermore, the infrared continuum would increase when dust forms (Dwek 1988*a*), so the steady decrease in the infrared flux for times less than 450 days (Roche *et al.* 1989; Wooden 1989) rules out the formation of significant amounts of dust at this epoch. Thus, virtually all the iron is still in the gaseous phase. For $t \sim 400$ days, Bregman *et al.* (1990) estimate that the fraction of stable nickel which is singly ionized is 0.8. This should also be a good estimate for the ionization fraction of iron, since the ionization ranges of these two species are similar (7.6–18.2 eV for [Ni II] and 7.9–16.2 eV for [Fe II]), and no doubly ionized iron or nickel is detected (Bregman *et al.* 1990). This suggests that there is about $M_{\rm Fe^+} = 0.8 \times 0.073 = 0.06\ M_\odot$ of Fe^+ at this epoch.

Using the collision strengths and Einstein A-values of Nussbaumer and Storey (1980, 1988), our [Fe II] transitions have critical densities for collisions with electrons of $n_{\rm cr} \lesssim 10^5$ cm^{-3} at temperatures $T \lesssim 10^4$ K. For an expansion velocity, $v \lesssim 5000$ km s^{-1}, the electron density at $t \sim 400$ days is $n_e \gg n_{\rm cr}$. Thus, the level populations follow a Boltzman distribution and are not determined by the ambient radiation field. If the transitions are optically thin, the line fluxes are proportional to the total number of ions in the upper level of the transition, and the measured line fluxes imply a unique iron mass. If some of

the emission is optically thick, the actual mass wil be larger than this estimate, which is then a minimum mass. Conversely, knowledge of the actual mass and the measured minimum mass allows an estimate of the average escape probability. Using the ground-state 26 μm line flux (because it is less temperature sensitive), a distance to the Large Magellanic Cloud of 55 kpc, and a temperature of 4400 K from the next section, we find that the minimum mass of singly ionized iron is $M_{\rm min}$ (26 μm) = 0.026 $M_\odot$. For an ionization fraction of 0.8, this is consistent with the optically thin iron mass of 0.033 $M_\odot$ deduced from lower resolution measurements at the same epoc by Dwek (1988*b*). The minimum mass changes by $\lesssim$25% when the assumed temperature is varied from 2000–5000 K. Since $M_{\rm min}$ (26 μm) < $M_{\rm Fe+}$, we infer that the 26 μm transition is not completely optically thin, but from equation (4) has an escape probability of β_{26} = [0.026/0.06] = 0.45. This corresponds to an average optical depth $\bar{\tau}_{26} \sim 2.0$. As discussed earlier, $\bar{\tau}_{26}$ is an average over the line profile function (McCray 1989). It cannot be understood as a spatial average over the nebula in any simple way, unless the density is constant, in which case τ is also constant throughout the nebula and equals $\bar{\tau}$.

c) Optical Depth Distribution

The line profiles carry a wealth of information regarding the velocity structure of the expanding remnant. For a physically thin, symmetric shell which is also optically thin, the high-velocity wings of the profile come from a small area centered on the shell; the blue wing arises from the ejecta which is approaching the observer, and the red wing arises from the ejecta which is receding. The low-velocity portions of the profile come from material in a ring at the outer edge of the shell that is ejected near the plane of the sky. In this case, the shape of the profile is rectangular (Bertout and Magnan 1987). In an "onion shell" model for the supernova, where the elements are ejected in a number of concentric, thin shells with the heavier elements interior to the lighter ones, the velocities of the heavier elements will be smaller, and thus their line profiles will be narrower.

In § IV*a* we argued, on the basis of the observed (large) line fluxes and the consequent low optical depths, that the iron in SN 1987A was actually ejected with a wide range of velocities. Assuming nearly spherical symmetry, the high-velocity emission in the wings of the profile still comes from small, approximately circular areas centered on the ejecta. However, the low-velocity emission in the center of the profile now includes contributions from the entire disk, since there is material with a low line-of-sight velocity along all lines of sight. Except for the extreme edges of the profiles, the emission at each velocity comes from throughout the nebula.

Hence, both optically thin and optically thick material may contribute to the emission at each velocity. We consider two simple limiting cases: (1) A one-component model in which the high–optical depth regions result from a smooth density distribution which varies with radius. (2) A two-component model that consists of high–optical depth clumps embedded in an optically thin interclump medium which has a smooth density distribution as a function of radius. As discussed below, the optically thick clumps are assumed to be sufficiently thick that they contribute negligibly to the observed emission. Cases (1) and (2) are constrained by the measured line fluxes to have similar average escape probabilities (eq. [4] and § IV*b*), but the global distribution of material can be quite different. In § V we compute detailed radiative transfer models for both cases.

The fact that the 26 μm flux at t = 400 days is within $-5\% \pm 24\%$ of its value at t = 250 days significantly constrains the optical depth distribution. The emission from optically thin regions will only change because of changes in the temperature, the iron ionization fraction, or the iron mass. We can estimate each of these effects. At $t \sim 270$ days, Moseley *et al.* (1989) find $T \sim 6000^{+2000}_{-1000}$ K and an iron ionization fraction $x_{\rm Fe+} \sim 0.85$. For T dropping from 6000 to 4400 K (§ IV*d*) at 400 days, the 26 μm flux would increase by only 13%. The drop in ionization fraction from $\sim$0.85 to $\sim$0.80 (Bregman *et al.* 1990) would lead to a flux decrease of 6%. Radioactive decay of cobalt would increase the iron mass by 9% from 250 to 400 days. Summing these changes, the flux from optically thin regions would be expected to increase by $\sim$15% from 250 to 400 days. On the other hand, if the size of the optically thick regions scales with source size, at constant temperature the line flux from these regions increases with the square of the time (e.g., Colgan and Hollenbach 1988), or a factor of 2.5 for this period. A drop in temperature from 6000 to 4400 K would decrease the optically thick brightness by $\sim\frac{3}{4}$, for a net increase in the optically thick emission by a factor of 1.9.

Our measurements limit the increase of the 26 μm line flux between t = 250 and t = 400 days to $\lesssim$20%, which shows that most of the emission must originate in optically thin regions. From equations (1) and (2), the optical depth of any region will decrease with the square of the time. For the smooth density distribution of case (1), we would have expected some material with $\tau \geq 1$ at 250 days to have become optically thin by 400 days, resulting in an increased line flux. However, the small change in flux indicates that there was little material at 250 days with $\tau \sim 1$. Thus there is either a very clumpy medium, like case (2), or the density gradient for case (1) is sufficiently steep that there was little material with $\tau \sim 1$ at 250 days.

The similarity of the 18 and 26 μm, profiles to the 1.26 μm [Fe II] profile at this epoch (Fig. 3) favors the clumping of case (2). We have argued that the 26 μm profile is produced by optically thin emission from $\sim$45% of the iron. For $T \sim 4400$ K, the optical depth of the 18 μm line is $\tau_{18} = 0.6\tau_{26}$, so the optical depth distribution of the two lines is similar. However, for an optical depth distribution like case (1), the [Fe II] transition at 1.26 μm should be optically thin throughout the ejecta. This means that an iron density profile which is centrally peaked at low velocities will contribute emission primarily in the core of the 1.26 μm line, producing a very different profile than that of the 18 μm line. Case (2), on the other hand, can produce similar profiles for these two transitions if the embedded clumps remain optically thick at 1.26 μm. A possibility we consider more likely is that the clumps are optically thin at 1.26 μm but have a spatial distribution which is nearly identical to that of the interclump material producing the 18 and 26 μm emission lines.

d) Temperature

In this section, we derive the temperature of the iron for various assumptions about the optical depth distribution. The upper level of the 18 μm transition is $\Delta E/k \sim 3000$ K above the ground state. Since $n_e \gg n_{\rm cr}$, the number of ions in the upper level of the 18 μm transition is related to the number of ions in the upper level of the 26 μm transition by the Boltzman equation. Thus, the ratio of the fluxes in the optically thin limit probes the temperature of the emitting regions. In this limit, our 26 and 18 μm fluxes yield a temperature $T \sim 6600^{+2800}_{-1700}$ K. A more accurate temperature can be obtained by excluding the

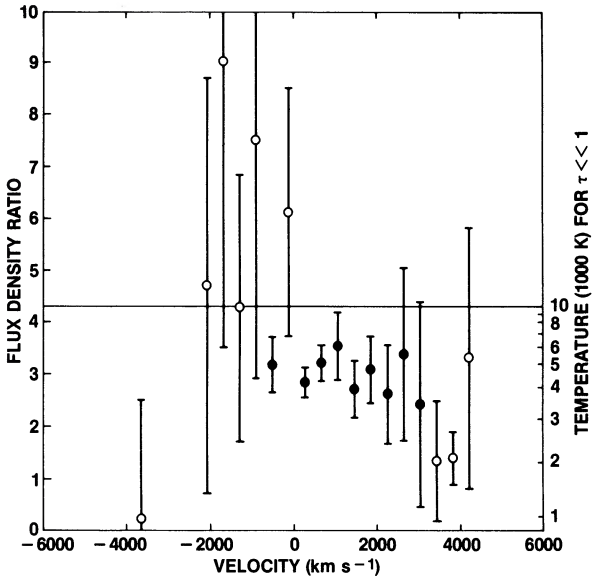

FIG. 4.—The 18 μm to 26 μm flux density ratio after removal of the continua. The temperature scale for the optically thin case is also shown. Points used to determine the average temperature are denoted by filled circles.

points in the profiles with large errors and examining the flux ratio as a function of velocity. The ratio of the two profiles with the continuum removed was computed and is shown in Figure 4. An error-weighted average of the temperatures with signal-to-noise ratios in excess of unity yields a mean temperature of 4400 ± 400 K with the assumption $\tau \ll 1$. This average excludes the high-velocity feature and thus spans the velocity range $-500 \leq v \leq 3000$ km s^{-1} (the nine filled circles in Fig. 4).

If the emission originates from regions with $\tau \gg 1$, the theoretical flux ratio would be ~ 4.3, with less than a 10% change as the temperature varies from 2000–5000 K. None of the observed ratios across the profile are significantly greater than 4.3, and many are significantly less, indicating that at most velocities the emission is not dominated by the contribution from optically thick regions, in agreement with the discussion in § IV*c*.

For intermediate cases with some optically thin and some optically thick material, the temperature corresponding to the measured flux ratio depends on the optical depth distribution. For our optical depth cases (1) and (2), where most of the emission comes from optically thin regions, the flux ratios are equal to those in the optically thin limit and $T \sim 4400$ K. The contribution of any optically thick emission to the line fluxes will result in the actual temperature being somewhat lower than this estimate. As discussed above, the fact that the 18 and 1.26 μm profiles are nearly identical (see Fig. 3) implies a fairly homogeneous temperature for the ejecta.

V. RADIATIVE TRANSFER MODELS

In § IV we showed that the observed line fluxes are clearly inconsistent with onion shell models in which each element expands at a nearly constant velocity with negligible shear. The material must have a large range of expansion velocities in order to account for the observations. To obtain information about the density and temperature structure of the expanding ejecta and to estimate the minimum expansion velocity of the iron, we have constructed a sphericaly symmetric model which predicts the [Fe II] line profiles from SN 1987A.

Specifically, our model generates profiles given the total mass of singly ionized iron, the temperature (assumed isothermal), the index α for the iron density n_{Fe^+} as a power-law function of radius r ($n_{Fe^+} = kr^{\alpha}$), and the minimum and maximum expansion velocities v_{min} and v_{max}, which correspond to the minimum and maximum radii of the iron shell. The model divides each line of sight through the ejecta into a number of volume cells. Starting from the backside of the ejecta, the emission is computed for each cell, attenuated by the optical depth of the foreground cells, and summed to form the spectrum for an individual line of sight. The contribution from all parallel lines of sight are then combined, assuming cylindrical symmetry, to produce the final spectrum.

There are several approximations and simplifications made: (1) As discussed in § III*a*, there is strong evidence for asymmetries in the expansion of SN 1987A. However, a symmetric model is justified as a first approximation because of the near symmetry of our profiles in the central ± 2500 km s^{-1}. (2) Since $n_e \gg n_{cr}$, the level populations of the iron depend only on the temperature. The temperature is determined by the balance between the heating due to the radioactive decay of ^{56}Co and the cooling due to optical emission lines (Colgan and Hollenbach 1988; Woosley 1988). The temperature is independent of the infrared radiation field and the level populations are, therefore, assumed to be decoupled from it. (3) For most of the model runs, the temperature is assumed isothermal. This is a reasonable assumption even for inhomogeneous densities, since both the heating and the cooling rates scale similarly with the iron density (Colgan and Hollenbach 1988). (4) Since shortly after the explosion, the acceleration of the ejecta has been much less than the initial acceleration so the expansion is approximated as homologous with velocity $v_{exp} = r/t$.

In fitting the 26 and 18 μm lines, we explored a grid of five parameters: density exponent α, velocities v_{min} and v_{max}, temperature T, and ionized iron mass M_{Fe^+}. For $2000 \lesssim T \lesssim 5000$ K, the best-fit parameters are insensitive to the exact temperature, so this parameter was fixed at $T = 4400$ K (§ IV*d*). Each model was compared with the data by adding the observed continuum levels to the computed Fe^+ profiles, calculating the χ^2 deviation per degree of freedom for each line, and then minimizing the sum of the two χ^2. The data points in the high-velocity feature ($v \sim +3900$ km s^{-1}) discussed in § III*b* were excluded from the fits. The mean redshift of each profile was treated as a free parameter; however, the χ^2 minimization procedure gave values nearly identical to those derived from Gaussian fits (Table 1). We have computed models corresponding to both cases (1) and (2) of § IV*c*, although as we discussed, other considerations favor the clumpy case (2).

To simulate the fraction of Fe^+ hidden in optically thick clumps for case (2), we used a singly ionized iron mass of $M_{Fe^+} = 0.03\ M_{\odot}$. The best fit gives $\chi^2 = 1.4$ for the 26 μm profile and $\chi^2 = 1.7$ for the 18 μm profile, with fit parameters $\alpha = -3.2 \pm 1.1$, $v_{min} = 650 \pm 650$ km s^{-1}, and $v_{max} \sim 15{,}000$ km s^{-1}. The "errors" given for the parameters are the range of values with the total χ^2 for both spectra increasing by $\lesssim 2$. The data, the best-fit model for case (2), and the residuals are shown in Figures 5*a* and 5*b*. The points excluded from the fit are noted by open circles. The fit to the 18 μm profile, particularly the blueshifted side, is somewhat high. This results from the fact that we are simultaneously fitting both transitions with the

same density profile, and the 18 μm profile has a blue-shifted wing extending to higher velocities. The model in Figure 5 is the best simultaneous fit to both profiles in a χ^2 sense.

To model case (1), where the average optical depth is due to a smooth variation of density with radius,we used the full mass of $M_{Fe^+} = 0.06\ M_\odot$, again with $T = 4400$ K. The best fit has $\chi^2 = 1.8$ for the 26 μm profile and $\chi^2 = 4.3$ for the 18 μm profile, with parameters $\alpha = -2.8 \pm 0.3$, $v_{min} = 0^{+500}_{-0}$ km s^{-1}, and an unphysically large v_{max}. Similar fits were obtained for the range of masses $0.05 \leq M_{Fe^+} \leq 0.07\ M_\odot$ with the same parameter ranges. The difficulty with the case (1) fits is that to obtain the correct total flux v_{min} must be quite small, and this leads to a profile which is narrower than observed; broader profiles contain too much flux.

The best-fit models for both cases (1) and (2) are consistent with the measured flux of the 26 μm line at 250 days (Paper I) to within the quoted errors. However, the power-law fit to the 18 μm profile for case (1) is significantly worse than for case (2), which suggests that the high–optical depth regions are probably in clumps rather than due to a smooth density distribution. Either model can fit the 1.26 μm integrated flux (Meikle *et al.* 1989) with some adjustment of the temperature ($T = 3700$ K for case [1] and $T = 4800$ K for case [2]). However, as discussed in § IV*c*, the clumpy case (2) gives a much better fit to the observed 1.26 μm line profile. Taken together, these arguments provide strong evidence for the existence of clumps which are optically thick at 26 μm and are distributed throughout the ejecta.

We have also considered some variations to our standard model in order to ascertain the sensitivity to various effects. First, we have fitted an exponential density distribution to our profiles. The best fits give $\chi^2 = 4.3$ for both lines with 0.03 $M_\odot$ of singly ionized iron (case [2]) and $\chi^2 > 10$ for both lines with 0.06 $M_\odot$ (case [1]). These fits are significantly worse than the corresponding best fits using power-law density distributions. Second, the larger line width of the higher excitation 18 μm transition—2900 km s^{-1} compared with 2500 km s^{-1} for the 26 μm transition—implies that the temperature may increase slightly with radius, in agreement with theoretical expectations (McCray 1989). A model fit for temperature increasing with radius was examined. The same mean temperature, $\bar{T} = 4400$ K averaged with respect to density, was employed. The fit to the two profiles did not improve significantly.

By examining the limits on the model parameters, we note that the best fits are not very sensitive to the minimum and maximum velocities, except that $v_{min} \ll 2000$ km s^{-1} $\ll v_{max}$. The maximum expansion velocity of 15,000 km s^{-1} that we found for case (2) is consistent with our earlier discussion, which showed that a significant fraction of the iron was accelerated to high velocities and mixed with overlying layers. However, our spectra only extend to ± 5000 km s^{-1}, so the evidence for these high velocities is rather weak, and we consider it unlikely that Fe^+ was actually accelerated to such velocities. The models are quite insensitive to the maximum velocity because the signal-to-noise is low in the wings of the profiles. The large maximum velocity in the model may simply reflect a high-velocity flattening out of the density profile relative to a power law.

The minimum expansion velocity is consistent with theoretical expectations of $v_{min} \lesssim 700$ km s^{-1} (e.g., Pinto and Woosley 1988*b*). It is related to the flat tops of the central profiles and to the total measured flux through the optical depth. Lower minimum velocities result in slightly lower line fluxes and larger maximum flux densities than are observed. The best-fit power-law models are consistent with an iron density profile

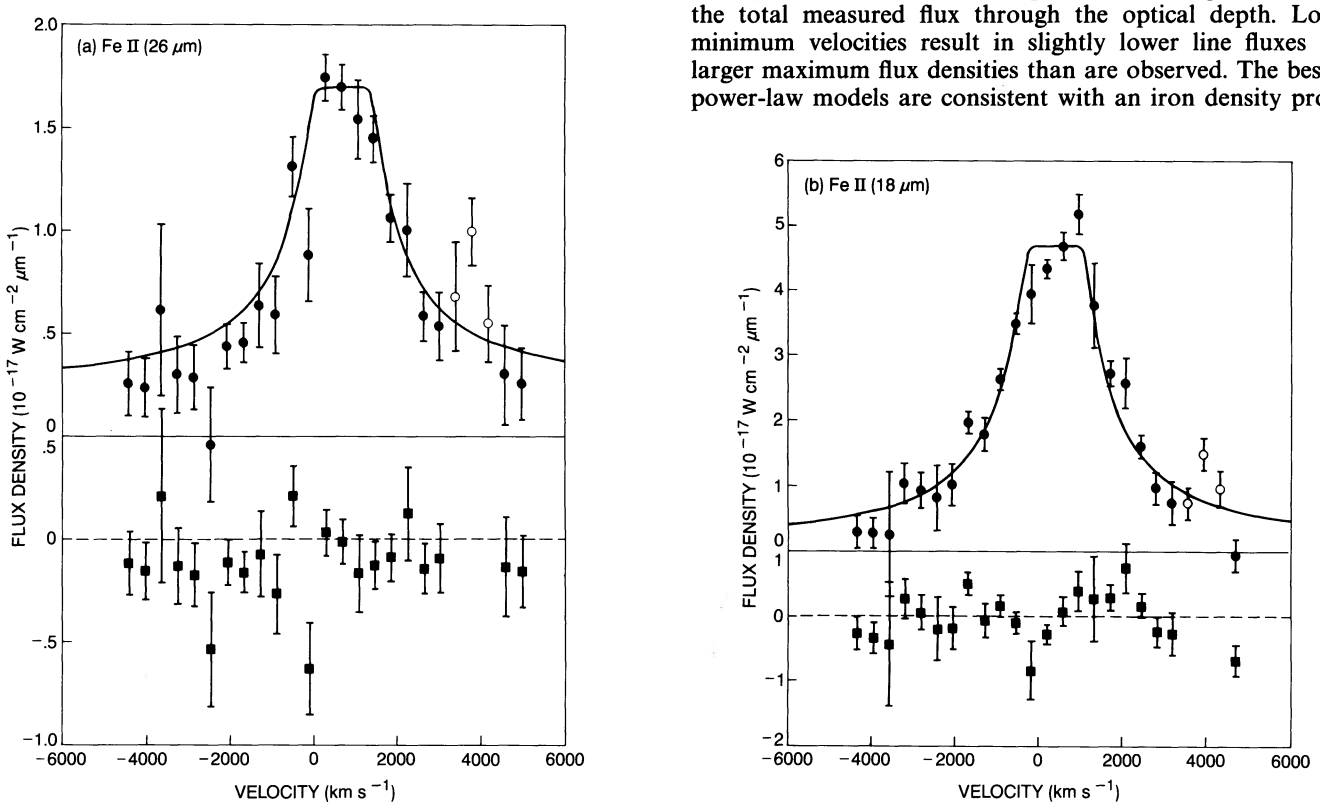

FIG. 5.—Comparison of the [Fe II] 26 μm (*a*) and 18 μm (*b*) spectra of SN 1987A with model spectra. The parameters of the model are $v_{min} = 650$ km s^{-1}, $v_{max} = 15{,}000$ km s^{-1}, $\alpha = -3.2$, $T = 4400$ K, and $M_{Fe^+} = 0.03\ M_\odot$. Points noted by filled circles are included in the fit. Residuals between the data and the fit are shown at the same scale below the spectra.

which varies as r^{-3}. The iron density profile is the product of the mass density and the mass fraction of singly ionized iron, both as functions of the expansion velocity. The 10HMM model of Pinto and Woosley (1988*a*, *b*) and Woosley, Pinto, and Weaver (1988), which fit the X-ray and γ-ray observations by allowing mixing of the Co and Fe to the outer layers of the mantle, have a roughly constant iron mass fraction for velocities $v \lesssim 2000$ km s^{-1}, while the density is decreasing over the same velocity range. In this case, our deduced Fe^+ distribution reflects the underlying density profile rather than the iron mass fraction as a function of velocity. Our result that $\alpha \sim -3$ is consistent, within the observational and theoretical uncertainties, with the density profile of the 10HMM model.

VI. SUMMARY

We have measured the [Fe II] profiles at 18 and 26 μm from SN 1987A with a resolution of $\sim$400 km s^{-1}. The central portion of each [Fe II] profile is well-fitted by a Gaussian with a FWHM of 2900 and 2500 km s^{-1}, respectively. The centroid velocity is redshifted relative to the LSR by 450 ± 200 km s^{-1} at 18 μm and by 680 ± 200 km s^{-1} at 26 μm. The central part of the 18 μm profile appears somewhat asymmetric. The asymmetry in the 26 μm line is not significant with our signal to noise. The integrated line fluxes alone imply a maximum expansion velocity of $v_{max} \gtrsim 2000$ km s^{-1} and a minimum expansion velocity $v_{min} \ll v_{max}$. The velocity extent of the emission demonstrates that a significant fraction of the iron has mixed with the overlying hydrogen regions. Between 4% and 17% of the iron has been accelerated to velocities relative to the velocity centroid of $|v - v_{cent}| > 3000$ km s^{-1}. In addition, there is a high-velocity emission feature at about +3500 km s^{-1} relative to the main emission peak which contains $\sim$3% of the total iron mass and has $T \sim 2600$ K. Although electron scattering in the hydrogen envelope may account for the redshift of the two Fe^+ profiles relative to the presupernova center of mass, it cannot account for either the high-velocity feature or the observed asymmetry in the 18 μm line profile. The most likely explanation for these asymmetries is an asymmetric distribution of Fe^+.

The measured 26 μm line flux corresponds to a total singly ionized iron mass of 0.026 $M_\odot$; this value is quite insensitive to the temperature of the emitting gas. This is less than the 0.07 $M_\odot$ of ^{56}Fe inferred from the preexisting iron and the decay of ^{56}Co which powers the light curve. Since the bulk of the iron is Fe^+, as deduced from infrared transitions of [Ni I], [Ni II], and [Ni III], we conclude that the mass difference implies that the [Fe II] lines are partially optically thick. Because of the similarity of the 18 and 1.26 μm (Spyromilio, Meikle, and Allen 1990) Fe^+ profiles and the small change in the 26 μm line flux from 250 days, the missing iron is probably hidden in regions of enhanced optical depth or "clumps," rather than in a smooth density distribution with higher optical depths at low velocities. This optical depth distribution implies a temperature of 4400 K.

The line fluxes and profiles are inconsistent with a physically thin shell of gas, either optically thin or optically thick, and they show that there is a wide range of expansion velocities for the iron. Spherically symmetric models of the ejecta profiles with an optically thin component containing 45% of the iron mass give best fits to the observed lines for the density decreasing with radius as $r^{-3.2 \pm 1.1}$ and a minimum velocity of 650 ± 650 km s^{-1}. The fits again suggest that the remaining material has high optical depth and is not part of a smooth density distribution, but rather is distributed in clumps throughout the ejecta.

We are pleased to acknowledge the continued efforts of the staff of the Kuiper Airborne Observatory and the support of NASA under UPN 352. We are grateful to Rockwell International, particularly M. Staeplebroek and K. Hayes, for the preparation and loan of the Si:As BIB detectors. We thank H. Moseley, R. Loewenstein, W. Glaccum, and R. Silverberg for freely discussing their spectra and calibration source fluxes during the expedition, thereby helping to assure the success of our observations. Discussions with P. Pinto and J. Spyromilio were helpful in improving this paper. We appreciate the comments of J. Bregman and M.-M. MacLow on the manuscript. Part of this work was done while S. W. J. C., S. D. L., and M. G. B. held National Research Council NASA Research Associateships at the Ames Research Center. S. W. J. C. also acknowledges support of NASA-Ames Research Center Interchange grant NCA 2-355.

REFERENCES

Aitken, D. K., Smith, C. H., James, S. D., Roche, P. F., Hyland, A. R., and McGregor, P. J. 1988*a*, *M.N.R.A.S.*, **231**, 7P.
———. 1988*b*, *M.N.R.A.S.*, **235**, 19P.
Arnett, D., Fryxell, B., and Müller, E. 1989, *Ap. J. (Letters)*, **341**, L63.
Bertout, C., and Magnan, C. 1987, *Astr. Ap.*, **183**, 319.
Bouchet, P., and Danziger, J. 1988, *IAU Circ.*, No. 4575.
Bregman, J. D., Axelrod, T. S., Cohen, M., Pinto, P. A., Rank, D. M., Witteborn, F. C., and Wooden, D. H. 1990, *Ap. J. (Letters)*, submitted.
Chevalier, R. A., and Soker, N. 1989, *Ap. J.*, **341**, 867.
Colgan, S. W. J., Haas, M. R., Erickson, E. F., Lord, S. D., and Hollenbach, D. J. 1990, *Bull. AAS.*, **21**, 1215.
Colgan, S. W. J., and Hollenbach, D. J. 1988, *Ap. J. (Letters)*, **329**, L25.
Corliss, C., and Sugar, J. 1982, *J. Phys. Chem. Ref. Data*, **11**, 135.
Cropper, M., Bailey, J., McCowage, J., Cannon, R. D., Couch, W. J., Walsh, J. R., Strade, J. O., and Freeman, F. 1988, *M.N.R.A.S.*, **231**, 695.
Dopita, M. A., *et al.* 1988, *A.J.*, **95**, 1717.
Dwek, E. 1988*a*, *Ap. J.*, **329**, 814.
———. 1988*b*, *Proc. Astr. Soc. Australia*, **7**, 468.
Ebisuzaki, T., Shigeyama, T., and Nomoto, K. 1989, *Ap. J. (Letters)*, **344**, L65.
Erickson, E. F., Haas, M. R., Colgan, S. W. J., Lord, S. D., Burton, M. G., Wolf, J., Holenbach, D. J., and Werner, M. 1988, *Ap. J. (Letters)*, **330**, L30 (Paper I).
Erickson, E. F., *et al.* 1984*a*, in *Symposium on Airborne Astronomy*, ed. H. Thronson and E. Erickson (NASA Conf. Publ. 2353), p. 133.
———. 1985, *Infrared Phys.*, **25**, 513.
Erickson, E. F., Matthews, S., Augason, G. C., Houck, J. R., Rank, D. M., and Haas, M. R. 1984*b*, *Proc. SPIE*, **509**, 129.
Fabian, A. C., and Rees, M. J. 1988, *Nature*, **335**, 50.
Fransson, C., and Chevalier, R. A. 1989, *Ap. J.*, **343**, 323.
Gehrz, R. D., and Ney, E. P. 1987, *Proc. Nat. Acad. Sci.*, **84**, 6961.
Gezari, D. Y., Schmitz, M., and Mead, J. M. 1987, *NASA Ref. Publ.* No. 1196.
Haas, M. R., Colgan, S. W. J., Erickson, E. F., Lord, S. D., and Burton, M. G. 1988, *IAU Circ.*, No. 4578.
Harvey, P. M., Hoffman, W. F., and Campbell, M. F. 1978, *Astr. Ap.*, **70**, 165.
Karovska, M., Koechlin, L., Nisenson, P., Papaliolios, C., and Standley, C. 1988, *IAU Circ.*, No. 4604.
McCray, R. 1989, in *Molecular Astrophysics*, ed. T. Hartquist (Cambridge: Cambridge University Press), pp. 439–458.
Meikle, W. P. S., Allen, D. A., Spyromilio, J., and Varani, G.-F. 1989, *M.N.R.A.S.*, **238**, 193.
Meikle, W. P. S., Matcher, S. J., and Morgan, B. L. 1987, *Nature*, **329**, 608.
Moseley, H., Dwek, E., Glaccum, W., Graham, J., Loewenstein, R., and Silverberg, R. 1988*a*, *IAU Circ.*, No. 4574.
———. 1988*b*, *IAU Circ.*, No. 4576.
Moseley, H., Glaccum, W., Loewenstein, R., Silverberg, R., Dwek, E., and Graham, J. 1987, *IAU Circ.*, No. 4500.
Moseley, S. H., Dwek, E., Glaccum, W., Graham, J. R., Loewenstein, R. F., and Silverberg, R. F. 1989, *Ap. J.*, **347**, 1119.
Nagasawa, M., Nakamura, T., and Miyama, S. M. 1988, *Pub. Astr. Soc. Japan*, **40**, 691.
Nisenson, P., Papaliolios, C., Karovska, M., and Noyes, R. 1987, *Ap. J. (Letters)*, **320**, L15.
Nussbaumer, H., and Storey, P. J. 1980, *Astr. Ap.*, **89**, 308.
———. 1988, *Astr. Ap.*, **193**, 327.

Pinto, P. A., and Woosley, S. E. 1988*a*, *Nature*, **333**, 534.
———. 1988*b*, *Ap. J.*, **329**, 820.
Rank, D. M., Bregman, J. D., Witteborn, F. C., Cohen, M., Lynch, D. K., and Russell, R. W. 1988*a*, *Ap. J. (Letters)*, **325**, L1.
Rank, D. M., Pinto, P. A., Woosley, S. E., Bregman, J. D., Witteborn, F. C., Axelrod, T. S., and Cohen, M. 1988*b*, *Nature*, **331**, 505.
Roche, P. F., Aitken, D. K., Smith, C. H., and James, S. D. 1989, *Nature*, **337**, 533.
Serabyn, E., Lacy, J. H., Townes, C. H., and Bharat, R. 1988, *Ap. J.*, **326**, 171.
Spyromilio, J., Meikle, W. P. S., and Allen, D. A. 1990, *M.N.R.A.S.*, submitted.
Spyromilio, J., Meikle, W. P. S., Learner, R. C. M., and Allen, D. A. 1988, *Nature*, **334**, 327.
Suntzeff, N. B., Hamuy, M., Martin, G., Gómez, A., and González, R. 1988, *A.J.*, **96**, 1864.
Wampler, E. J., and Richichi, A. 1989, *Astr. Ap.*, **217**, 31.
Whitelock, P. A., *et al.* 1988, *M.N.R.A.S.*, **234**, 5P.
Witteborn, F., Bregman, J., Wooden, D., Pinto, P., and Rank, D. 1988, *IAU Circ.*, No. 4592.
Witteborn, F. C., Bregman, J. D., Wooden, D. H., Pinto, P., Rank, D. M., and Cohen, M. 1989, *Ap. J. (Letters)*, **338**, L9.
Wood, P. R., Nulsen, P. E. J., Gillingham, P. R., Bessell, M. S., Dopita, M. A., and McCowage, C. 1989, *Ap. J.*, **339**, 1073.
Wooden, D. H. 1989, Ph.D. thesis, University of California at Santa Cruz.
Woosely, S. E. 1988, *Ap. J.*, **330**, 218.
Woosley, S. E., Pinto, P. A., and Ensman, L. 1988, *Ap. J.*, **324**, 466.
Woosley, S. E., Pinto, P. A., and Weaver, T. A. 1988, *Proc. Astr. Soc. Australia*, **7**, 355.

MICHAEL G. BURTON, SEAN W. J. COLGAN, EDWIN F. ERICKSON, MICHAEL R. HAAS, and STEVEN D. LORD: NASA-Ames Research Center, MS: 245-6, Moffett Field, CA 94035-1000

DAVID J. HOLLENBACH: NASA-Ames Research Center, MS: 245-3. Moffett Field, CA 94035-1000